International Journal of Fluid Power, 2015
Vol. 16, No. 2, 99–110, http://dx.doi.org/10.1080/14399776.2015.1064663

Taylor & Francis
Taylor & Francis Group

Bilateral teleoperation of a pneumatic actuator: experiment and stability analysis

N. Garmsiri[a], Y. Sun[a], C. Yang[b] and N. Sepehri[a]*

[a]*University of Manitoba, Winnipeg, Manitoba, Canada R3T-5V6;* [b]*University of North Dakota, Grand Forks, ND 58202-8359, USA*

(*Received 1 February 2015; accepted 18 June 2015*)

This paper presents design, implementation and stability analysis of a bilateral teleoperated pneumatic actuation system whereby a low-cost pneumatic actuator is navigated by an operator using a commercially-available haptic device. The actuator is subject to an external force, the value of which is scaled and rendered on the haptic device to provide the operator with a feeling of the interaction at the remote site. Sliding mode control scheme is implemented for positioning the pneumatic actuator. The performance of the system is experimentally evaluated through several experiments including interaction with springs having different stiffnesses and an arbitrary resistive/assistive force applied by a human at the actuator side. Stability of the entire system is theoretically proven using the concept of Lyapunov exponents that quantitatively measures convergence/divergence of initially infinitely close solution trajectories.

Keywords: pneumatic actuator; bilateral teleoperation; sliding mode control; stability analysis; Lyapunov exponents

1. Introduction

Bilateral teleoperated robotic systems are becoming more popular in many applications from carrying hazardous materials (Kontz and Book 2007) to microsurgery (Le *et al*. 2013). A bilateral system is composed of a master manipulator, operated by human and a slave manipulator to emulate the motion of the master. Information about the force applied to the slave by the environment is sent to the master to provide the operator with the feeling as if she/he is directly operating at the remote site. Master and slave communicate through a communication channel and a central controller (Kontz and Book 2007).

A major issue in bilateral systems is stability (Zarei-nia and Sepehri 2012). The overall bilateral system should be stable irrespective of the input command. Stable interaction between the environment and the teleoperated slave manipulator is not always guaranteed due to unstructured external force. Network delay between the master and the slave is another potential reason of instability. Therefore, theoretical stability analysis is required for the bilateral systems.

Using a pneumatic actuator as the slave manipulator makes bilateral teleoperation more challenging. Positioning of a pneumatic actuator is difficult due to friction and compressibility of air. Nevertheless, the use of pneumatics offers several advantages. Pneumatic actuators are cost-effective, clean and easy to maintain. Moreover, they are good candidates to work as rehabilitation robots due to the compressibility of air, which makes them able to absorb unwanted forces (Morales *et al*. 2011).

As far as bilateral control of pneumatic manipulators is concerned, research in this area is limited to a few studies. A pneumatic slave manipulator driven by solenoid on/off valves was designed to follow the motion of an identical pneumatic master manipulator, and sliding mode control (SMC) was used as the positioning method (Hodgson *et al*. 2012, Leleve *et al*. 2012, Le *et al*. 2013). Stability analysis was done on this system based on the Hannaford closed-loop model of bilateral systems (Hannaford 1989), which assumes a linear model for the combination of the master and the slave manipulators (Leleve *et al*. 2012). Using linear models may not be desirable because they do not include the complexity of nonlinear pneumatic actuators. Further studies on the stability of the same platform were conducted using SMC condition for stability, considering the external force as model uncertainty (Hodgson *et al*. 2012). This assumption is not always recommended, especially when the interaction with the environment changes the model structure, e.g. the order of system (Hogan and Buerger 2004). A pneumatic slave actuator was navigated by an identical pneumatic master actuator in a bilateral way (Durbha and Li 2009). Stability was guaranteed by ensuring that the system was energetically passive (Khalil 1995) and considering that the environment was also passive (Hogan 1989). The same approach was implemented for navigating a pneumatically powered rescue crawler using a phantom haptic device (Durbha and Li 2010). Simulations and limited experiments in free motion were presented. A pneumatic artificial muscle was also controlled by a haptic device as the master manipulator (Li *et al*. 2012). An estimation of the external force was reflected as feedback using the impedance model of the slave manipulator.

In this paper, we present construction, experimental evaluation and stability analysis of a low-cost pneumatic

*Corresponding author. Email: nariman.sepehri@umanitoba.ca

actuator coupled with a commercially-available haptic device in bilateral mode. SMC scheme is implemented for robust position tracking of the pneumatic actuator in the presence of model uncertainties and disturbances. The external force experienced by the slave actuator is reflected to the operator by the built-in internal controller of the master manipulator. Experimental evaluations include arbitrary resistive/assistive force applied by a human at the actuator side. Experiments, while important, only validate stability of the control system for a limited number of trajectories; it is desirable to theoretically prove stability of the developed bilateral pneumatic system for a wide range of trajectories. Although Lyapunov direct method is the most common approach of stability analysis in nonlinear systems, construction of Lyapunov function for an already-designed control system is difficult if not impossible (Yang *et al*. 2012). The concept of Lyapunov exponents (LEs) has been successfully used for stability study of industrial systems such as control of a hydraulic manipulator (Sekhavat *et al*. 2005) and balance control of a biped robot (Yang *et al*. 2012, Sun and Wu 2013). It is believed to be a powerful alternative for stability analysis of nonlinear systems which cannot be analyzed using Lyapunov direct method. Thus, another objective of this paper is to introduce, for the first time, the novel application of the concept of LEs to the stability analysis of bilateral pneumatic systems. This approach facilitates the separation process of controller design and stability analysis.

The rest of this paper is organized as follows. The experimental setup, modeling of the system and the control scheme are described in Section 2. Section 3 shows simulation studies followed by stability analysis of the proposed bilateral pneumatic system using the concept of LEs in Section 4. Section 5 presents experimental results followed by conclusions.

2. Experimental setup and modeling

The experimental setup is shown in Figure 1. It consists of a PHANTOM® haptic devise as the master manipulator, a PC equipped with QUANSER® data acquisition board as the control station and a one degree-of-freedom sliding pneumatic actuator as the slave manipulator interacting with the environment. The above devices are connected to a local network with a constant and almost negligible delay. The pneumatic actuator setup has a double rod actuator with a 40 mm bore, 16 mm diameter rod and 500 mm stroke and is operated by a three-way five-port proportional directional flow control valve. The control station receives the position of the haptic device and sends a control signal to the valve to move the pneumatic actuator according to the movement of the master manipulator. The control station also receives data from the force sensor and renders it to the haptic device. The sampling frequency is 500 Hz. A handle is attached to the end of the actuator to facilitate interaction with a human at the actuator side.

Referring to Figure 1(a), the combined dynamics of the master manipulator and the human arm, in one dimension, is described as follows (Aliaga *et al*. 2004):

$$m_m\ddot{x}_m + b_m\dot{x}_m + k_m x_m = F_h + F_m \tag{1}$$

In Equation (1), m_m is the combined inertia of the master manipulator and human arm, b_m is the combined viscous coefficient of the master manipulator and the human arm and k_m is the combined stiffness of the master manipulator and the human arm. F_h is the force generated by the operator's hand and x_m is the displacement of the master. F_m is the control signal to the master manipulator indicating the force applied to the operator's hand; it is proportional to the external force experienced by the slave manipulator.

Referring to Figure 1(b), equation of motion for the actuator is given below:

$$M\ddot{x}_s = A(P_1 - P_2) + F_{\text{ext}} - (F_f + B\dot{x}_s) \tag{2}$$

where x_s denotes the position of the slave manipulator, M is the combined mass of the piston–rod assembly, A is the annulus area of the piston and, P_1 and P_2 are the absolute pressures in each of the actuator chambers. The external force from the environment is F_{ext}. B is the viscous friction coefficient regarding the viscous friction force. The dry friction, F_f is presented using LuGre friction model (Canudas de Wit *et al*. 1995) excluding the term related to viscous friction (Note that the viscous friction is included as a separate term in Equation (2)):

$$F_f = \sigma_0 z + \sigma_1 \dot{z} \tag{3}$$

In (3), σ_0 and σ_1 correspond to equivalent spring coefficient and equivalent damping coefficient of bristle in LuGre friction model, respectively. To find z, the following equation should be solved:

$$\dot{z} = \dot{x}_s - \frac{\sigma_0 |\dot{x}_s| z}{F_c + (F_s - F_c)e^{-(\dot{x}_s/v_{sv})^2}} \tag{4}$$

where F_c is the Coulomb friction, F_s is the static friction and v_{sv} is the Stribeck velocity.

To position the actuator, chamber pressures are varied by charging or discharging appropriate volumes of air. The differential equations relating the chamber pressures to the air mass flows, $\dot{m}_1$ and $\dot{m}_2$, are expressed as (Karpenko and Sepehri 2006):

$$\dot{P}_1 = \gamma RT\frac{\dot{m}_1}{V_1} - \alpha\gamma A\frac{\dot{x}_s P_1}{V_1} \tag{5}$$

$$\dot{P}_2 = -\gamma RT\frac{\dot{m}_2}{V_2} + \alpha\gamma A\frac{\dot{x}_s P_2}{V_2} \tag{6}$$

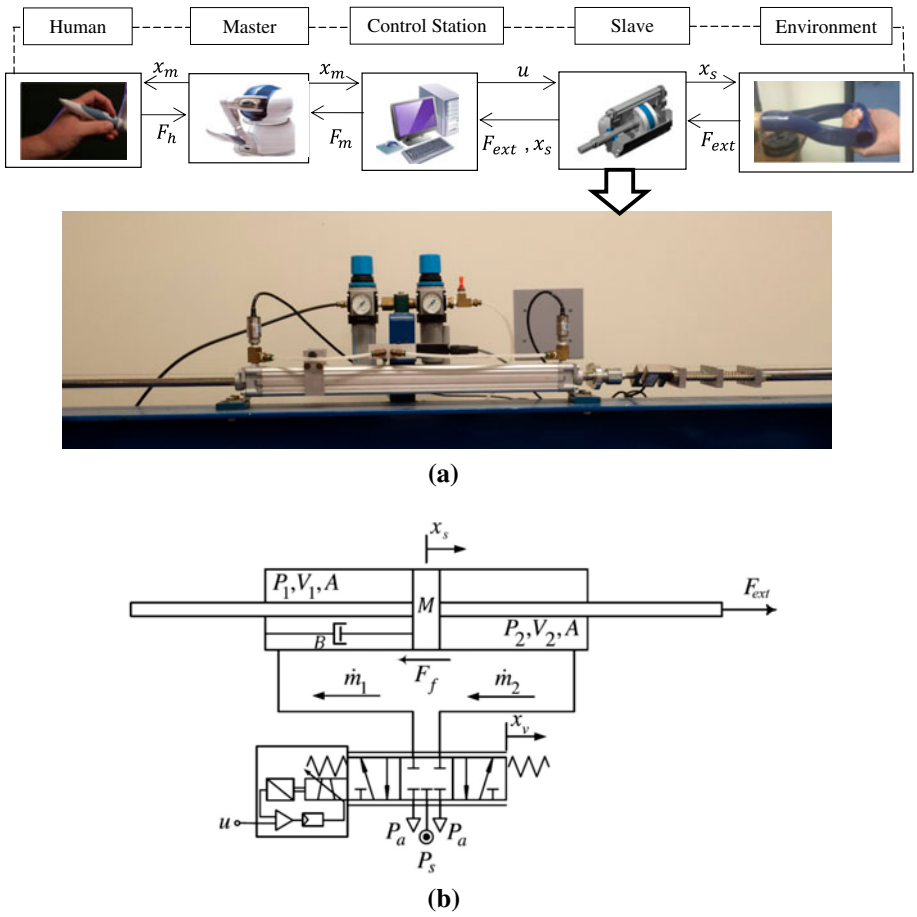

Figure 1. (a) Setup of bilateral control of pneumatic actuator; (b) schematic diagram of valve-controlled pneumatic actuator.

$$V_1 = V_0 + Ax_s \tag{7}$$

$$V_2 = V_0 + A(L - x_s) \tag{8}$$

In Equations (5) and (6), R is the ideal gas constant, γ is the ratio of specific heat and T is air temperature. α is known as compressibility flow correction factor (Karpenko and Sepehri 2006). V_1 and V_2 are the instantaneous air volumes at each of the chambers and depend on the position of the actuator as expressed in (7) and (8). V_0 corresponds to cylinder inactive volume and L is the actuator stroke. Defining $\bar{\gamma} = \sqrt{\gamma(2/(\gamma+1))^{(\gamma+1)/(\gamma-1)}/R}$, the nonlinear equations governing the mass flow rates of air through each control valve orifice are (Sanville 1971):

$$\begin{cases} \dot{m}_1 = wx_v\varnothing_1 \\ \dot{m}_2 = wx_v\varnothing_2 \end{cases} \tag{9}$$

where w and x_v are the orifice area gradient and the displacement of the valve spool, respectively. $\varnothing_i (i = 1,\ 2)$ is the mass flow per area unit, expressed as (Karpenko and Sepehri 2006):

$$\begin{cases} \varnothing_1 = \begin{cases} \frac{CP_s}{\sqrt{T}}\bar{\gamma}, & \frac{P_1}{P_s} \le b \\ \frac{CP_s}{\sqrt{T}}\bar{\gamma} \times \sqrt{1-\left(\frac{P_1/P_s - P_{cr}}{1-P_{cr}}\right)^{\frac{\gamma-1}{\gamma}}}, & \frac{P_1}{P_s} > b \end{cases} \\ \varnothing_2 = \begin{cases} \frac{CP_2}{\sqrt{T}}\bar{\gamma}, & \frac{P_a}{P_2} \le b \\ \frac{CP_2}{\sqrt{T}}\bar{\gamma} \times \sqrt{1-\left(\frac{P_a/P_2 - P_{cr}}{1-P_{cr}}\right)^{\frac{\gamma-1}{\gamma}}}, & \frac{P_a}{P_2} > b \end{cases} \end{cases} x_v \ge 0$$

$$\begin{cases} \varnothing_1 = \begin{cases} \frac{CP_1}{\sqrt{T}}\bar{\gamma}, & \frac{P_a}{P_1} \le b \\ \frac{CP_1}{\sqrt{T}}\bar{\gamma} \times \sqrt{1-\left(\frac{P_a/P_1 - P_{cr}}{1-P_{cr}}\right)^{\frac{\gamma-1}{\gamma}}}, & \frac{P_a}{P_1} > b \end{cases} \\ \varnothing_2 = \begin{cases} \frac{CP_s}{\sqrt{T}}\bar{\gamma}, & \frac{P_2}{P_s} \le b \\ \frac{CP_s}{\sqrt{T}}\bar{\gamma} \times \sqrt{1-\left(\frac{P_2/P_s - P_{cr}}{1-P_{cr}}\right)^{\frac{\gamma-1}{\gamma}}}, & \frac{P_2}{P_s} > b \end{cases} \end{cases} x_v < 0$$

In (10), C is the control valve coefficient of discharge, P_a is the atmospheric pressure, P_s is the supply pressure and b is the valve critical pressure ratio. The equation describing displacement of the valve spool given control signal, u, is:

$$\dot{x}_v = \frac{1}{\tau}(-x_v + K_v u) \tag{11}$$

where τ is the valve first-order time constant and K_v is the valve spool position gain. The parameters of the test rig, described by the above equations, are shown in Table 1. The rationality of choosing their values has been reported in (Aliaga *et al*. 2004, Karpenko and Sepehri 2006).

To provide the control signal for positioning the pneumatic actuator, SMC scheme is used. SMC is a robust control approach which provides consistent control performance in the presence of model uncertainties (Jouppila *et al*. 2014). It is known as the most common position controller for pneumatic actuators because of its robustness property (Al-Dakkan *et al*. 2006, Bone and Ning 2007, Gulati and Barth 2009). The integral sliding surface, used in this work, is adopted from the work by Shen (2010):

$$S = \left(\frac{d}{dt} + \delta\right)^3 \int_0^t e d\tau \tag{12}$$

where δ is a positive constant known as the control bandwidth and e is the position error defined as:

$$e = x_s - x_m \tag{13}$$

The SMC control law consists of two components: an equivalent control component, Av_{eq}, which is derived using the system dynamic model and, a robust control component, Av_{rb}, which compensates for the model uncertainties in order to provide a robust control law (Shen 2010):

$$u = (Av_{eq} + Av_{rb})/(wK_v) \tag{14}$$

The dynamics of the sliding surface can be written as (Khalil 1995):

$$\dot{S} = 0 \tag{15}$$

which gives the following expression:

$$Av_{eq} = \frac{\dddot{x}_m - \delta^3 e - 3\delta^2 \dot{e} - 3\delta \ddot{e} - Fx}{Px} \tag{16}$$

The associated variables Px and Fx are derived as:

$$Px = \frac{\gamma RTA}{M}\left(\frac{\varnothing_1}{V_1} + \frac{\varnothing_2}{V_2}\right) \tag{17}$$

$$Fx = -\frac{K\dot{x}_s + B\ddot{x}_s + \dot{F}_f - \dot{F}_{ext}}{M} \tag{18}$$

where

$$K = \alpha\gamma A^2\left(\frac{P_1}{V_1} + \frac{P_2}{V_2}\right) \tag{19}$$

Detailed derivation of the above equations are presented in (Shen 2010). The time rate of the change of dry friction, F_f is slow in comparison to the dynamics of system. Therefore, $\dot{F}_f$ can be considered negligible in Equation (18). Neglecting dry friction is mentioned in the previous application of SMC in positioning pneumatic actuators (Wu *et al*. 2004, Al-Dakkan *et al*. 2006, Gulati and Barth 2009). Since this simplification contributes to uncertainty, the robust part of SMC will take more effort to compensate for the simplification. Av_{rb} is formulated as follows:

Table 1. Parameters of pneumatic actuator (Aliaga *et al*. 2004, Karpenko and Sepehri 2006).

Parameter	Symbol	Value
Cylinder inactive volume	V_0 (m^3)	1.64×10^{-4}
Piston annulus area	A (cm^2)	10.6
Actuator stroke	L (m)	0.5
Total mass of actuator's moving parts	M (kg)	1.91
Valve coefficient of discharge	C	0.7
Valve critical pressure ratio	b	0.2
Pressure–volume work correction factor	α	1.2
Ratio of specific heat	γ	1.4
Ideal gas constant	R (J/kg K)	287
Temperature of air source	T (K)	300
Valve spool position gain	K_v (mm/V)	0.25
Valve first-order time constant	τ (ms)	4.2
Atmospheric pressure	P_a (Pa)	10^5
Supply pressure	P_S (Pa)	5×10^5
Valve orifice area gradient	w (mm^2/mm)	22.6
Viscous friction coefficient	B (Ns/m)	70
Coulomb friction	F_c (N)	32.9
Static friction	F_s (N)	38.5
Stribeck velocity	v_{sv} (m/s)	0.02
Equivalent spring coefficient of bristle	σ_0 (N/m)	4500
Equivalent damping coefficient of bristle	σ_1 (Ns/m)	93.13
Inertia of haptic and arm	m_m (kg)	0.4
Viscous coefficient of haptic and arm	b_m (Ns/m)	5
Stiffness of haptic and arm	k_m (N/m)	1000

$$Av_{\mathrm{rb}} = \frac{-K_{\mathrm{rb}}}{Px} sign(S) \tag{20}$$

where K_{rb} is a robustness gain. For practical purposes, the discontinuous *sign* function is approximated by continuous hypertangant function as follows:

$$sign(S) \approx \tanh(aS) \tag{21}$$

where a is a sufficiently large positive number.

3. Simulation studies

Simulation analysis is conducted to provide better understanding of the performance of the bilateral system described above. As shown in Figure 1, the bilateral system has two inputs: the force of the operator's hand applied to the master, F_h and the external force imposed to the slave from the environment, F_{ext}. The environment is assumed to be spring-dominant in the simulation; thus, F_{ext} will be proportional to the displacement of the slave:

$$F_{\mathrm{ext}} = -K_{\mathrm{ext}} x_s \tag{22}$$

In Equation (22), K_{ext} is the stiffness coefficient of the environment. The system has two control signals. The first one is the control signal to the master manipulator, F_m, which is proportional to the external force experienced by the slave manipulator:

$$F_m = K_{fs} F_{\mathrm{ext}} \tag{23}$$

In (23) K_{fs} is a scaling factor. The second control signal, u, positions the slave manipulator; it's value is determined by Equation (14).

Figure 2 shows the simulation results at the master side. The force of the operator's hand, F_h is considered to be constant and equal to 1 N as shown in Figure 2(a). Considering $K_{fs} = 0.01$ and $K_{\mathrm{ext}} = 100$ N/m, the force applied to the operator's hand is shown in Figure 2(b). The displacement of the master caused by the combination of F_h and F_m is shown in Figure 2(c). Figure 2(d) shows the external force.

Figure 3 shows the plots of variables coresponding to the slave manipulator. The controller parameters are $\delta = 60$ rad/s and $K_{\mathrm{rb}} = 3000$ m/s^3. The value of a in Equation (21) is chosen as 10^4. It is seen in Figure 3(a) that the slave reasonably follows the motion of the master and handles the external force fairly well. The position error shown in Figure 3(b) converges to zero as a result of the integral part of SMC. The chattering observed in x_s is caused by the robust part of SMC. The air pressure in each chamber is shown in Figure 3(c). Figure 3(d) shows the control signal. It should be noted that the control signal is in [0V 10V] range. A 5 V control signal means the valve is closed. The simulation shows that the entire bilateral system is stable and acts fast.

4. Stability analysis

The concept of LEs is employed here. This approach has been previously used for studying stability of nonlinear systems (Sekhavat *et al.* 2005, Sun and Wu 2013). LEs identify the asymptotic behaviour of nonlinear systems by observing the growth of two nearby orbits in the state space. The sign of LEs shows the stability of the system. A positive exponent indicates a chaotic behaviour. A system is considered stable if all of the exponents are non-positive. If all of the exponents are negative (i.e. the nearby orbits are convergent to each other), the system is exponentially stable and the basin of attraction is a fixed point. Zero exponents indicate that the nearby orbits, in one direction, neither converge nor diverge but stay in

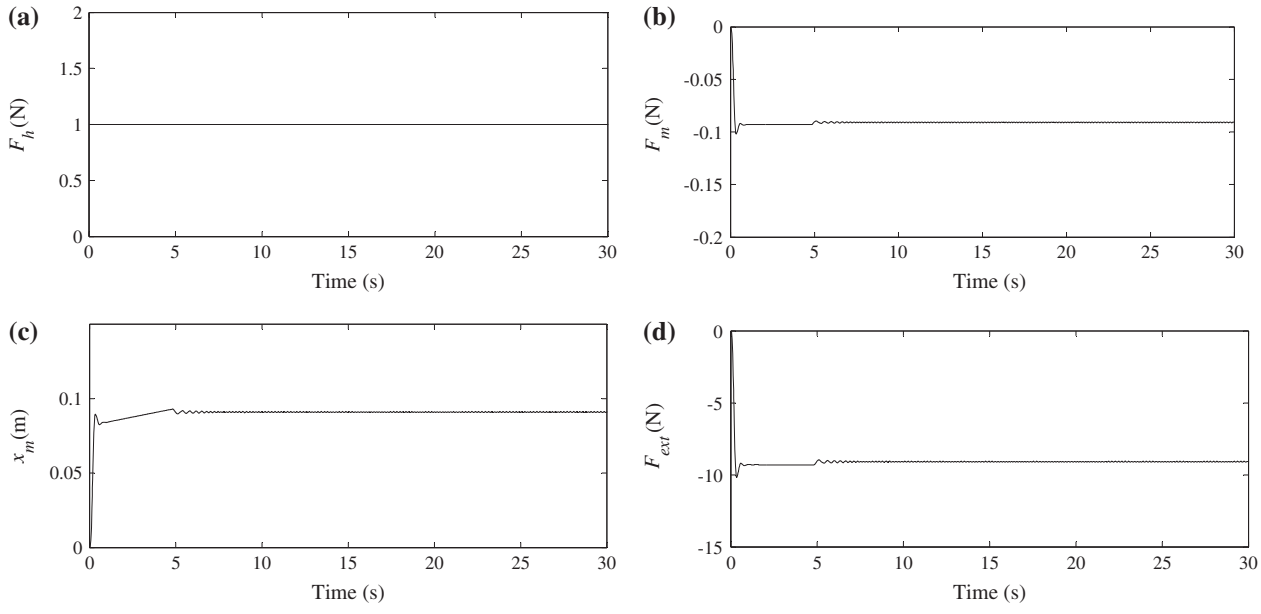

Figure 2. Simulation results of bilateral step tracking task: (a) force of operator's hand; (b) force of master manipulator; (c) displacement of master manipulator; (d) external force.

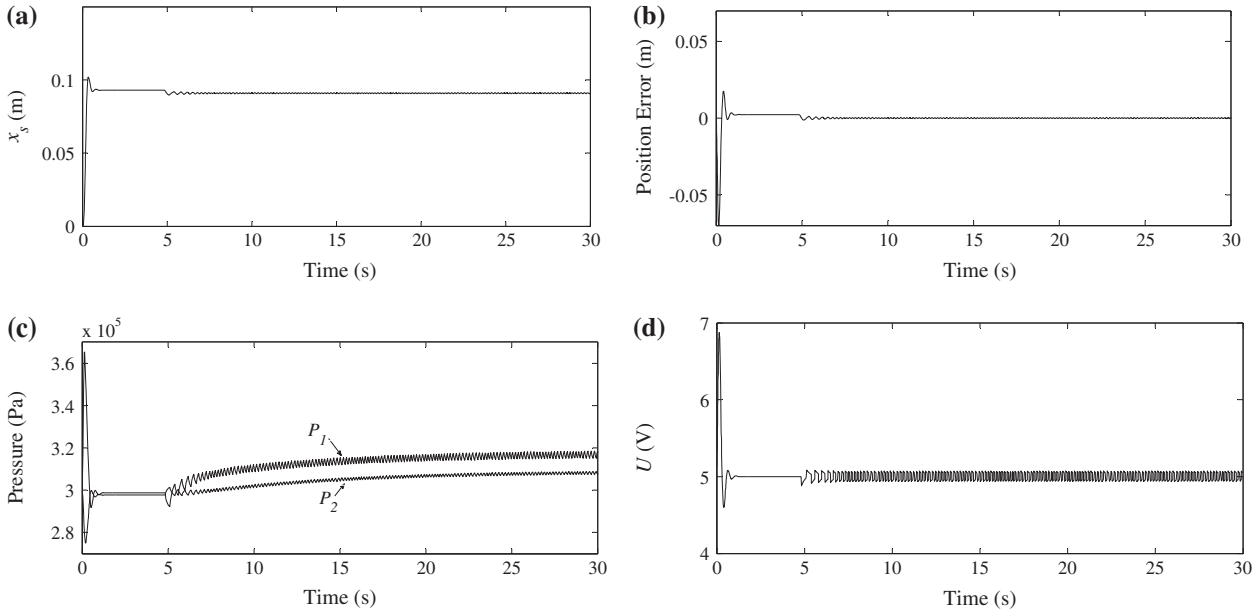

Figure 3. Simulation results of bilateral step tracking task: (a) displacement of slave manipulator; (b) tracking error between master and slave, $e = x_s - x_m$; (c) chamber pressures; (d) control signal.

fixed distance from each other. A dynamic system with one zero exponent while the others are negative is stable and the basin of attraction is one-dimensional (Sadri and Wu 2013).

It is crucial to note that LEs are 'invariant' measures of dynamic behaviour of a system. It means although one fiducial trajectory is chosen for calculation of LEs, as explained further in Appendix 1, the consequence of a Theorem of Oseledec (1968) proves that Lyapunov exponents are global properties of the dynamic systems and guarantee stability for any fiducial trajectory.

4.1. Calculation of LEs

A smooth dynamic system in an n-dimensional state space is considered:

$$\dot{x} = f(x) \tag{24}$$

where $x \in \mathbb{R}^n$, is the state vector with the initial value $x(0) = x_0$ and $f(x)$ is a continuous and differentiable function. A 'fiducial' trajectory is formed by integrating Equation (24) on the initial condition. Then, by defining orthogonal principal axes on the fiducial trajectory and observing the growth of each principal axis as time evolves, the asymptotic behaviour of the nonlinear system is identified. In discrete space, the ith ($i = 1, \ldots, n$) LE, λ_i is calculated by the formulation introduced by Wolf *et al.* (1985):

$$\lambda_i(t) = \frac{1}{T} \ln \frac{\delta x_i(t)}{\delta x_i(t_0)} \tag{25}$$

where δx_i is the length of a the ith principal axis of the infinitesimal n-dimensional hyper-ellipsoid and T is the time of the observance. The final numerical value of LE is calculated by the following equation (Wolf *et al.* 1985):

$$\lambda_i = \lim_{t \to \infty} \frac{1}{t} \ln \frac{\delta x_i(t)}{\delta x_i(t_0)} \tag{26}$$

Figure 4 shows the infinitesimal 2-dimensional hyper-ellipsoid. It is obvious that the lengths and directions of the principal axes change over the time.

To calculate the length of the ith principal axis, a linearized equations of motion is derived using the Jacobian matrix as follows:

$$\dot{\psi}_{x(t)} = F(x(t))\psi_{x(t)} \tag{27}$$

where

$$F(x(t)) = \left.\frac{\partial f(x)}{\partial x^T}\right|_{x=x(t)} \tag{28}$$

The principal axes are the columns of the solution matrix of Equation (27). In any iteration, the principal axes should be made orthogonal to avoid them from laying on close directions. For this reason, the Gram-Schmidt scheme (Wolf *et al.* 1985) is included in the calculation procedure.

The algorithm of calculating LEs repeats until the LEs converge to their true values (Yang *et al.* 2012). Then, the sign of LEs are used to study the stability of the dynamic

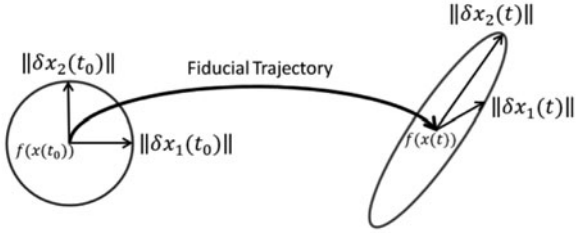

Figure 4. Evolutional of principal axes for a 2-dimensional system.

system in Equation (24). To provide better understanding of the algorithm of calculating LEs, stability of a simple dynamic system is analyzed in Appendix 1.

4.2. Stability verification

The stability of the system described in Section 3 is now studied. The state space model of bilateral pneumatic system is formed by defining the state space vector as

$$\vec{x} = [x_1 \quad x_2 \quad x_3 \quad x_4 \quad x_5 \quad x_6 \quad x_7 \quad x_8 \quad x_9]^T \tag{29}$$

where x_s is the displacement of the slave, $\dot{x}_s$ is the velocity of the slave, P_1 and P_2 are air pressures, x_v is the displacement of the spool and z is average bristle deflection in friction model. e, $\dot{e}$ and $\int_0^t e\mathrm{d}\tau$ are the position error as defined in Equation (13), its first derivative and integral, respectively. Considering Equations (13) and (29), one can see

$$x_m = x_1 - x_8 \tag{30}$$

Using the state variables in (29) and Equations (1)–(11), the state space model is constructed as:

$$\begin{cases} \dot{x}_1 = x_2 \\ \dot{x}_2 = \dfrac{1}{M}\left[A(x_3 - x_4) - K_{\text{ext}}x_1 - F_f - Bx_2\right] \\ \dot{x}_3 = +\gamma RT\dfrac{wx_5\varnothing_1}{V_0 + Ax_1} - \dfrac{\alpha\gamma Ax_2x_3}{V_0 + Ax_1} \\ \dot{x}_4 = -\gamma RT\dfrac{wx_5\varnothing_2}{V_0 + A(L - x_1)} + \dfrac{\alpha\gamma Ax_2x_4}{V_0 + A(L - x_1)} \\ \dot{x}_5 = \dfrac{1}{\tau}(-x_5 + K_v u) \\ \dot{x}_6 = x_2 - \dfrac{\sigma_0|x_2|x_6}{F_c + (F_s - F_c)e^{-(x_2/v_{sv})^2}} \\ \dot{x}_7 = x_8 \\ \dot{x}_8 = x_9 \\ \dot{x}_9 = \dfrac{A}{M}(x_3 - x_4) - \dfrac{1}{M}\left(K_{\text{ext}}x_1 + F_f + Bx_2\right) \\ \qquad - \dfrac{1}{m_m}\left(F_h - K_{fs}K_{\text{ext}}x_1\right) + \dfrac{b_m}{m_m}(x_2 - x_9) \\ \qquad + \dfrac{k_m}{m_m}(x_1 - x_8) \end{cases} \tag{31}$$

The dry friction is expressed in the state space as follows:

$$F_f = \sigma_0 x_6 + \sigma_1 x_2 - \frac{\sigma_0\sigma_1|x_2|x_6}{F_c + (F_s - F_c)e^{-(x_2/v_{sv})^2}} \tag{32}$$

To achieve the control signal in the state space model, Equations (16) and (20) are substituted into (14):

$$u = \frac{\dddot{x}_m - \delta^3 x_8 - 3\delta^2 x_9 - 3\delta\ddot{e} - Fx}{wK_vPx} + \frac{-K_{\text{rb}}\tanh(aS)}{wK_vPx} \tag{33}$$

The associated variables in Equation (33) are:

$$\dddot{x}_m = \frac{-K_{fs}K_{\text{ext}}}{m_m}x_2 - \frac{b_m}{m_m^2}(F_h - K_{fs}K_{\text{ext}}x_1) + \left(\frac{b_m^2}{m_m^2} - \frac{k_m}{m_m}\right)(x_2 - x_9) + \frac{b_m k_m}{m_m^2}(x_1 - x_8) \tag{34}$$

$$\ddot{e} = \frac{A}{M}(x_3 - x_4) - \frac{1}{M}\left(F_f + Bx_2\right) + K_{\text{ext}}\left(\frac{K_{fs}}{m_m} - \frac{1}{M}\right)x_1 + \frac{b_m}{m_m}(x_2 - x_9) + \frac{k_m}{m_m}(x_1 - x_8) - \frac{F_h}{m_m} \tag{35}$$

$$Fx = -\frac{\alpha\gamma A^2}{M}\left(\frac{x_3}{V_0 + Ax_1} + \frac{x_4}{V_0 + A(L - x_1)}\right)x_2 - \frac{K_{\text{ext}}}{M}x_2 - \frac{B}{M^2}(A(x_3 - x_4) - K_{\text{ext}}x_1 - Bx_2 - F_f) \tag{36}$$

$$S = \ddot{e} + 3\delta x_9 + 3\delta^2 x_8 + \delta^3 x_7 \tag{37}$$

$$Px = \gamma RTA\left(\frac{\varnothing_1}{V_0 + Ax_1} + \frac{\varnothing_2}{V_0 + A(L - x_1)}\right) \tag{38}$$

The mass flow rate per unit area is written in terms of state space variables defined in Equation (29):

$$\begin{cases} \varnothing_1 = \begin{cases} \dfrac{CP_s}{\sqrt{T}}\bar{\gamma}, & \dfrac{x_3}{P_s} \le b \\ \dfrac{CP_s}{\sqrt{T}}\bar{\gamma} \times \sqrt{1 - \left(\dfrac{x_3/P_s - P_{cr}}{1 - P_{cr}}\right)^{\frac{\gamma-1}{\gamma}}}, & \dfrac{x_3}{P_s} > b \end{cases} \\ \varnothing_2 = \begin{cases} \dfrac{Cx_4}{\sqrt{T}}\bar{\gamma}, & \dfrac{P_{\text{a}}}{x_4} \le b \\ \dfrac{Cx_4}{\sqrt{T}}\bar{\gamma} \times \sqrt{1 - \left(\dfrac{P_a/x_4 - P_{cr}}{1 - P_{cr}}\right)^{\frac{\gamma-1}{\gamma}}}, & \dfrac{P_{\text{a}}}{x_4} > b \end{cases} \end{cases} x_5 \ge 0$$

$$\begin{cases} \varnothing_1 = \begin{cases} \dfrac{Cx_3}{\sqrt{T}}\bar{\gamma}, & \dfrac{P_{\text{a}}}{x_3} \le b \\ \dfrac{Cx_3}{\sqrt{T}}\bar{\gamma} \times \sqrt{1 - \left(\dfrac{P_{\text{a}}/x_3 - P_{cr}}{1 - P_{cr}}\right)^{\frac{\gamma-1}{\gamma}}}, & \dfrac{P_{\text{a}}}{x_3} > b \end{cases} \\ \varnothing_2 = \begin{cases} \dfrac{Cx_3}{\sqrt{T}}\bar{\gamma}, & \dfrac{x_4}{P_s} \le b \\ \dfrac{Cx_3}{\sqrt{T}}\bar{\gamma} \times \sqrt{1 - \left(\dfrac{x_4/P_s - P_{cr}}{1 - P_{cr}}\right)^{\frac{\gamma-1}{\gamma}}}, & \dfrac{x_4}{P_s} > b \end{cases} \end{cases} x_v < 0 \tag{39}$$

Table 2. Values of Lyapunov exponents for bilateral step tracking task.

λ_1	0.0
λ_2	0.0
λ_3	−0.13
λ_4	−0.14
λ_5	−5.34
λ_6	−5.35
λ_7	−46.19
λ_8	−46.26
λ_9	−228.57

Having the initial condition $\vec{x}_0 = [0,\ 0,\ 3\times10^5,\ 3\times10^5,\ 0,\ 0,\ 0,\ 0,\ 0]^T$, the basin of attraction of Equation (31) is:

$$\begin{cases} x_2^{ss} = x_5^{ss} = x_7^{ss} = x_8^{ss} = x_9^{ss} = 0 \\ x_1^{ss} = \frac{F_h}{K_{\text{ext}}K_{fs}+K_m} \\ A(x_3^{ss} - x_4^{ss}) - k_{\text{ext}}x_1^{ss} - \sigma_0 x_6^{ss} = 0 \end{cases} \quad (40)$$

The LEs for the bilateral pneumatic system are calculated through integration of Equations (27) and (31) and then calculation of the exponents from (26). The solution analysis for the nonlinear and linearized equations is detailed in Appendix 1. The final numerical values of LEs are given in Table 2. Note that LEs are theoretically derived as $t \to \infty$. However, in numerical calculations we need to determine the exponents on a finite time interval. Particularly, when the largest LE of the system is zero, calculations should be continued long enough to ensure the system's largest exponent does not change afterwards. For the system under study, calculations were continued for 5000 s.

With respect to Table 2, the signs of LEs determine the stability characteristics of the dynamic system. If all of the exponents are negative, the dynamic system is exponentially stable. A zero exponent indicates no change in the magnitude of a principal axis. The number of zeros shows the dimension of the attractor (Sekhavat *et al*. 2005) e.g. a system with one zero exponent while other exponents are negative has a one-dimensional attractor (Sadri and Wu 2013). By revisiting Equation (40) one can see that the system has a set of equilibrium points where x_1^{ss}, x_2^{ss}, x_5^{ss}, x_7^{ss}, x_8^{ss} and x_9^{ss} will eventually have fixed values as time grows. However, a combination of x_3^{ss}, x_4^{ss} and x_6^{ss} must satisfy the following equation:

$$A(x_3^{ss} - x_4^{ss}) - K_{\text{ext}}x_1^{ss} - \sigma_0 x_6^{ss} = 0 \quad (41)$$

Having three unknowns (x_3^{ss}, x_4^{ss}, x_6^{ss}) and one Equation in (41), the solution of (40) is a 2-dimensional plane. Therefore, the basin of attraction of Equation (31) is 2-dimensional. This fact justifies the two zero LEs observed in Table 2, since the number of zeros should be equal to the number of the dimension of the basin attraction (Sekhavat *et al*. 2005, Sadri and Wu 2013). The values of LEs in Table 2 clearly proves that the entire control system is stable despite friction, external force, chattering and replacement of non-smooth *sign* functions with smooth hyperbolic tangent functions.

5. Experimental evaluation

Experiments were conducted to study the performance of the bilateral pneumatic system. In the first test, the master manipulator was moved periodically and the slave manipulator followed this movement. A spring was mounted in front of the slave manipulator in order to generate an external force proportional to actuator displacement. The stiffness of spring was approximately

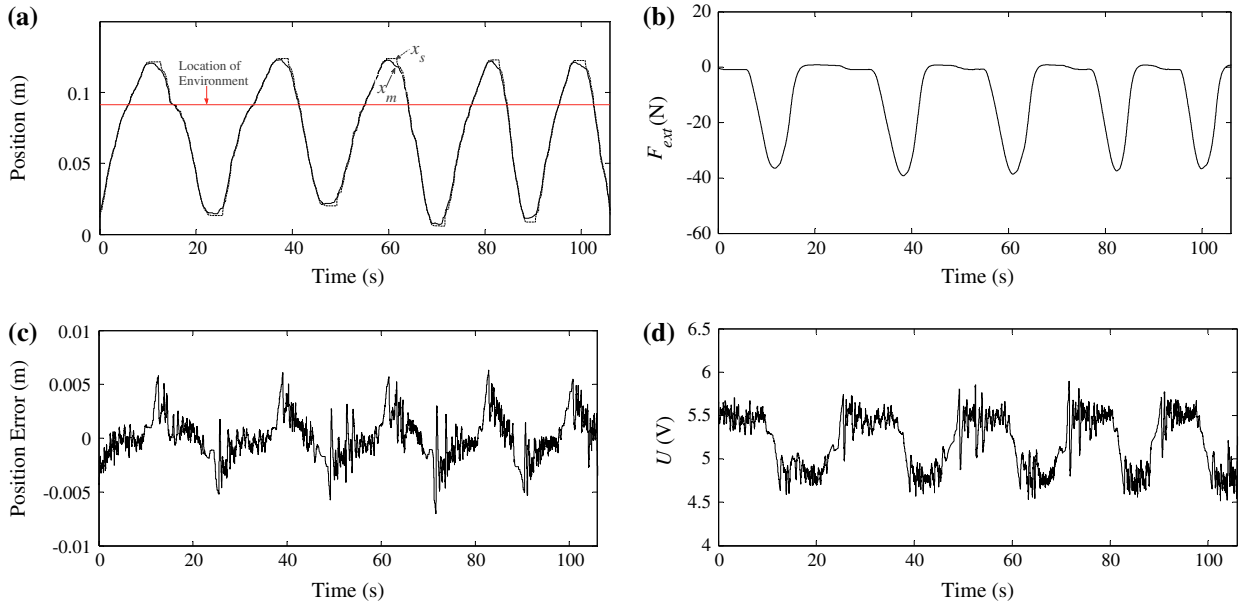

Figure 5. Experimental results of periodic tracking while interacting with a soft spring: (a) tracking response; (b) external force; (c) position error between master and slave; (d) actuator controller output.

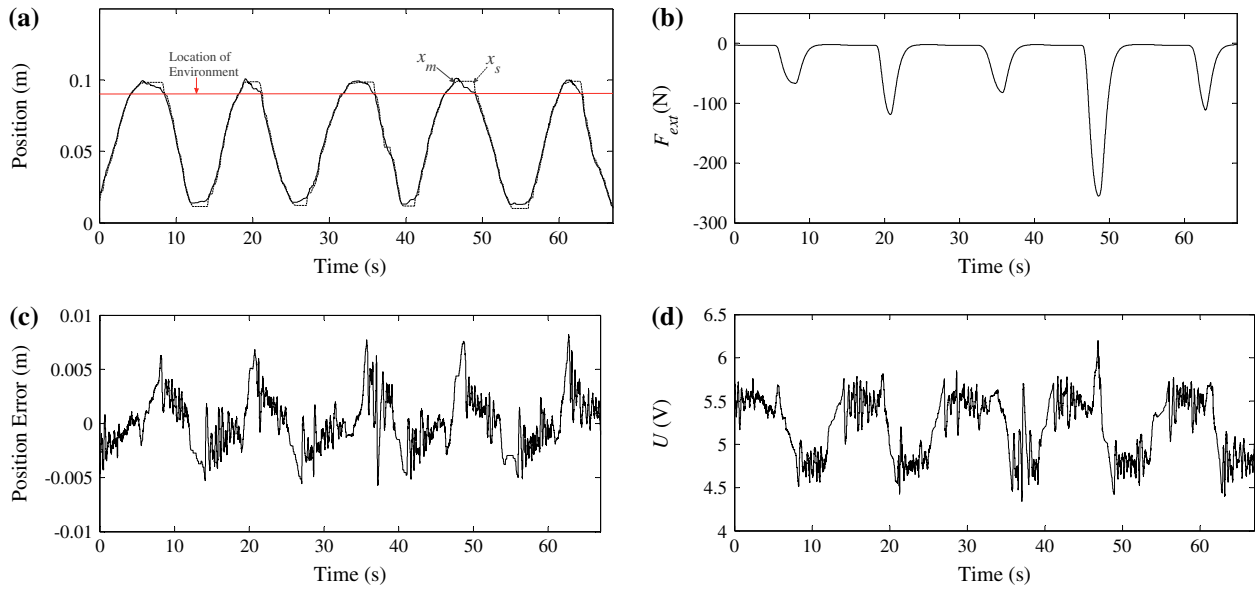

Figure 6. Experimental results of periodic tracking while interacting with a stiff spring: (a) tracking response; (b) external force; (c) position error between master and slave; (d) actuator controller output.

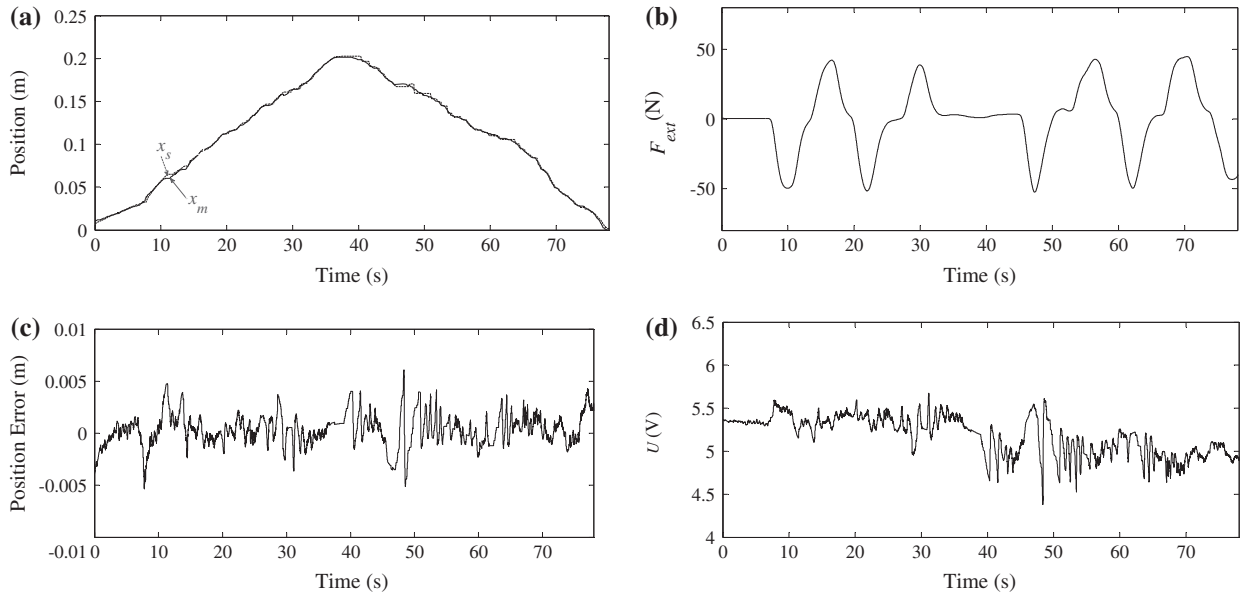

Figure 7. Experimental results of haptic-navigated tracking task while interacting with an arbitrary resistive-assistive external force applied to the actuator: (a) tracking response; (b) external force; (c) position error between master and slave; (d) actuator controller output.

1.2 kN/m. The experiment started by moving the actuator in free space, then making a contact with spring and applying a force. This is to also examine the performance of the system in transition between the two states. Figure 5(a) shows the displacement of the master and the slave manipulators in the presence of external force that is shown in Figure 5(b). Figure 5(c) shows an adequate tracking quality. The control signal generated by SMC, and shown in Figure 5(d), is unsaturated and reasonable. The chattering of the control signal is due to the robust part of the SMC. As mentioned before, the control signal varies between 0 and 10 V; a 5 V control signal corresponds to the valve being in the neutral (closed) position.

A similar bilateral tracking task was repeated with a spring of 10 kN/m stiffness. Figure 6(a) shows the displacement of the master and the slave manipulators. The external force was higher than the previous experiment

as shown in Figure 6(b). The external force was rendered to the operator's hand which provided a feeling about the distant environment. Subsequently, the operator could decide to move the haptic device further. The control signal is shown in Figure 6(d). This test shows that the bilateral system maintains the performance in dealing with the stiff environment.

In the next test, the slave was subject to a variable external force. Figure 7(a) shows the position tracking of the master and the slave. As shown in Figure 7(b), the external force with the maximum magnitude of 70 N was repeatedly imposed to the slave by a human in both resistive and assistive directions. Figure 7(d) shows the control signal. These experiments further confirm that the proposed bilateral pneumatic system works stably for various tracking tasks and different external force profiles.

Conclusion

A teleoperated pneumatic system was constructed using a haptic device as the master and a pneumatic cylinder as the slave manipulator. The goal was to arrive at a bilateral system capable of dealing with different environmental interactions while performing a tracking task. Sliding mode controller was employed for positioning the pneumatic actuator. The interaction force was reflected to the operator by the master device via the built-in controller. The performance of the control system was evaluated experimentally using scenarios involving various environmental effects, namely, soft and stiff spring forces, and arbitrary forces generated directly by a human at the slave side. Experimental results showed that the controlled pneumatic system satisfied position tracking and handled the external force well. Furthermore, for the first time, the stability of the proposed control system was theoretically proven using the concept of LEs.

Disclosure statement

No potential conflict of interest was reported by the authors.

Funding

This work was supported by NSERC-Discovery Grant [grant number RGPIN 121353-2013].

ORCID

N. Garmsiri http://orcid.org/0000-0002-9399-4969

References

Al-Dakkan, K., Barth, E., and Goldfarb, M., 2006. Dynamic constraint-based energy-saving control of pneumatic servo systems. *Journal of dynamic systems, measurement, and control*, 128 (3), 655–662.

Aliaga, I., Rubio, A., and Sanchez, E., 2004. Experimental quantitative comparison of different control architectures for master-slave teleoperation. *IEEE transactions on control systems technology*, 12 (1), 2–11.

Bone, G. and Ning, S., 2007. Experimental comparison of position tracking control algorithms for pneumatic cylinder actuators. *IEEE/ASME transactions on mechatronics*, 12 (5), 557–561.

Canudas de Wit, C., Olsson, H., Astrom, K., and Lischinsky, P., 1995. A new model for control of systems with friction. *IEEE transactions on automatic control*, 40 (3), 419–425.

Durbha, V. and Li, P.Y., 2009. Passive bilateral teleoperation and human power amplification with pneumatic actuators. *In*: *Proceedings of the ASME 2009 dynamic systems and control conference*, 12–14 October, Hollywood, CA, 863–870.

Durbha, V. and Li, P.Y., 2010. Passive tele-operation of pneumatic powered robotic rescue crawler. *In*: *Proceeding of 6th FPNI-PhD symposium*, 15–19 June, West Lafayette, IN, 451–466.

Filippov, A., 1960. Differential equations with discontinuous right-hand sides. *Math Sbornnik*, 51, 99–128 [English Translation: American Mathematical Society Translations, 42, 199–231, 1964].

Filippov, A., 1988. *Differential equations with discontinuous right-hand sides*. Dordrecht, ND: Kluwer Academic Publishers.

Gulati, N. and Barth, E., 2009. A globally stable, load-independent pressure observer for the servo control of pneumatic actuators. *IEEE/ASME transactions on mechatronics*, 14 (3), 295–306.

Hannaford, B., 1989. A design framework for teleoperators with kinesthetic feedback. *IEEE transactions on robotics and automation*, 5 (4), 426–434.

Hodgson, S., Le, M., Tavakoli, M., and Pham, M., 2012. Improved tracking and switching performance of an electro-pneumatic positioning system. *Mechatronics*, 22, 1–12.

Hogan, N., 1989. Controlling impedance at the man/machine interface. *In*: *Proceeding of IEEE international conference on robotics and automation*, 14–19 May, Scottsdale, AZ, 1626–1631.

Hogan, N. and Buerger, S.P., 2004. Impedance and Interaction Control. Chapter 19. *In*: *Robotics and automation handbook*. New York, NY: CRC Press, 1–24.

Jouppila, V., *et al.*, 2014. Sliding mode control of a pneumatic muscle actuator system with a PWM strategy. *International journal of fluid power*, 15 (1), 19–31.

Karpenko, M. and Sepehri, N., 2006. Development and experimental evaluation of a fixed-gain nonlinear control for a low-cost pneumatic actuator. *IEE proceedings of control theory and applications*, 153 (6), 629–640.

Khalil, H., 1995. *Nonlinear systems*. Upper Saddle River, NJ: Prentice Hall.

Kontz, M. and Book, W., 2007. Flow control for coordinated motion and haptic feedback. *International journal of fluid power*, 8, 13–23.

Kunze, M., 2000. *Non-smooth dynamical systems*. Berlin: Springer-Verlag.

Leleve, A., Pham, M.T., Tavakoli, M., and Moreau, R., 2012. Towards delayed teleoperation with pneumatic master and slave for MRI. *In*: *ASME 11th biennial conference on engineering systems design and analysis*, July 2–4, Nantes, 837–846.

Le, M., *et al.*, 2013. Bilateral control of nonlinear pneumatic teleoperation system with solenoid valves. *IEEE transaction on control systems technology*, 21 (4), 1463–1470.

Li, H., Tadano, K., and Kawashima, K., 2012. Achieving force perception in master-slave manipulators using pneumatic

artificial muscles. *In*: *SICE annual conference*, 20–23 August, Akita, 342–1345.
Morales, R., Badesa, F.J., Garcia-Aracil, N., Sabater, J.M., and Perez-Vidal, C., 2011. Pneumatic robotic systems for upper limb rehabilitation. *Journal of medical & biological engineering & computing*, 49 (10), 1145–1156.
Müller, P., 1995. Calculation of Lyapunov exponents for dynamic systems with discontinuities. *Chaos, solitons & fractals*, 5 (9), 1671–1681.
Oseledec, V., 1968. A multiplicative ergodic theorem: Lyapunov characteristic numbers for dynamical system. *Transaction of Moscow math society*, 19, 197–231.
Sadri, S. and Wu, C., 2013. Stability analysis of a nonlinear vehicle model in plane motion using the concept of Lyapunov exponents. *International journal of vehicle mechanics and mobility*, 51 (6), 906–924.
Sanville, F.E., 1971. A new method of specifying the flow capacity of pneumatic fluid power valves. *In*: *BHRA 2nd international fluid power symposium*, Guildford, 37–47.
Sekhavat, P., Sepehri, N., and Wu, C.Q., 2005. Overall stability analysis of hydraulic actuator's switching contact control using the concept of Lyapunov exponents. *In*: *Proceedings of the IEEE international conference on robotics and automation*, 18–22 April, Barcelona, 550–556.
Shen, X., 2010. Nonlinear model-based control of pneumatic artificial muscle servo systems. *Control engineering practice*, 18, 311–317.
Sun, Y. and Wu, C., 2013. Stability analysis via the concept of Lyapunov exponents: a case study in optimal controlled biped standing. *International journal of control*, 85 (12), 1952–1966.
Wolf, A., Swift, J., Swinney, H., and Vastano, J., 1985. Determining Lyapunov exponents from a time series. *Journal of physica*, 16 (4), 285–317.
Wu, J., Goldfarb, M., and Barth, E., 2004. On the observability of pressure in a pneumatic servo actuator. *Journal of dynamic systems, measurement, and control*, 126, 921–924.
Yang, C., Wu, C., and Zhang, P., 2012. Estimation of Lyapunov exponents from a time series for n-dimensional state space using nonlinear mapping. *Nonlinear dynamics*, 69, 1493–1507.
Zarei-nia, K. and Sepehri, N., 2012. Lyapunov stable displacement-mode haptic manipulation of hydraulic actuators: theory and experiment. *International journal of control*, 85 (9), 1313–1326.

Appendix 1. Procedure of calculating Lyapunov exponents

Consider a nonlinear mass-spring-damper described below:

$$\tilde{M}\ddot{x} + \tilde{B}\dot{x} + \tilde{K}x^2 = F(x) \tag{A.1}$$

where x is the position of the spring. $\tilde{M}$, $\tilde{B}$ and $\tilde{K}$ are inertia, damping and stiffness coefficients and $F(x)$ is the force defined as

$$F(x) = K_p(X_d - x) \tag{A.2}$$

X_d is the desired position and K_p is a positive coefficient. The state space model of the nonlinear mass spring damper is shown as follows:

$$\dot{x} = \begin{cases} \dot{x}_1 = x_2 \\ \dot{x}_2 = \frac{1}{\tilde{M}}(F(x) - \tilde{B}\dot{x} - \tilde{K}x^2) \end{cases} \tag{A.3}$$

Assuming $\tilde{M} = 0.1$, $\tilde{B} = 5$, $\tilde{K} = 15$, $K_p = 50$ and $X_d = 1$, to calculate the LEs for (A.3), first, we should find the linearized equation.

$$\dot{\psi}_{x(t)} = \begin{bmatrix} 0 & 1 \\ -\frac{2\tilde{K}x_1x_2 + K_p}{\tilde{M}} & -\frac{\tilde{B}}{\tilde{M}} \end{bmatrix} \psi_{x(t)} \tag{A.4}$$

Considering initial condition $x^0 = [0 \quad 0]$ and $\psi^0 = \begin{bmatrix} 1 & 0 \\ 0 & 1 \end{bmatrix}$, the iterative algorithm of calculating LEs is as follows:

Step 1: Integrate (A.3) and (A.4) over a time step. After $T = 0.01$ s, we have

$$x^1 = [0.0212 \quad 3.9009] \tag{A.5}$$

$$\psi^1 = \begin{bmatrix} 0.2383 & 0.9499 \\ -1.5777 & -3.6920 \end{bmatrix} \tag{A.6}$$

Step 2: Apply Gram-Schmidt method to make the principal axes of ψ^1 orthogonal in order to find the relevant growth of each principal axis of the infinitesimal 2-dimensional hyper-ellipsoid:

$$\psi^{1,\text{orthogonal}} = \begin{bmatrix} 0.2383 & 0.3834 \\ -1.5777 & 0.0579 \end{bmatrix} \tag{A.7}$$

Step 3: Calculate LEs:

$$\lambda_1^1(t) = \frac{1}{0.01}\ln\frac{\begin{bmatrix} 0.2383 \\ -1.5777 \end{bmatrix}}{\begin{bmatrix} 1 \\ 0 \end{bmatrix}} = 91.23 \tag{A.8}$$

$$\lambda_2^1(t) = \frac{1}{0.01}\ln\frac{\begin{bmatrix} 0.3834 \\ 0.0579 \end{bmatrix}}{\begin{bmatrix} 0 \\ 1 \end{bmatrix}} = -569.88 \tag{A.9}$$

Step 4: Normalize the principal axes:

$$\psi^{1,\text{normal}} = \begin{bmatrix} 0.1494 & 0.9888 \\ -0.9888 & 0.1494 \end{bmatrix} \tag{A.10}$$

Step 5: Consider x^1 and $\psi^{1,\text{normal}}$ as initial condition; repeat steps 1 to 4.

After 100 s, the numerical values of LEs are determined to be $\lambda_1 = -13.25$ and $\lambda_2 = -34.75$. Since they are negative, the system described in (A.3) is stable.

Appendix 2. Linearization and solution analysis

The required conditions for validity of applying the concept of LEs are firstly the existence of solution for nonlinear system should be proven; secondly, the linearized equation should have a unique solution. One should also be able to linearize the nonlinear system in order to find the Jacobian matrix (Sekhavat *et al*. 2005); these conditions are studied here for the system (31) that is under investigation.

I. Solution analysis for nonlinear equation

Let region $\Omega = R^n \times R$ and let D be an arbitrary compact set in Ω. The right-hand side of (31) is measurable, and bounded by $B(t)$, which is obviously integrable on D. Thus, the right-hand side of (31) satisfies Filippov's solution theory (Filippov 1988) and according to that, for an arbitrary initial condition $x(t_0) = a$, where $(t_0, a) \in \Omega$, a solution for Equation (31) exists which satisfy the above initial condition.

II. Solution analysis for linearized equation

The existence and uniqueness of the solution of the linearized equations of motion (27) is addressed using the theory of Caratheodory for differential equations (Filippov 1988). According to this theory, since all the elements of the linearized equations of motion are defined and piecewise continuous in x, and measurable, and $|F(x(t)) \leq m(t)|$, where the function $m(t)$ is summable on each finite interval, the solution of (27) with arbitrary initial condition $\psi_t(t_0) = \psi_{t_0}(t \in [t_0, t_f])$ exists on the whole interval $[t_0, t_f]$ and is unique.

III. Linearization of dynamic model at nonsmooth instants

With respect to Equation (31), the nonlinear equations of motion cannot be linearized at the following instants: (i) $x_2 = 0$, in friction model described by Equation (32); (ii) $\frac{P_d}{P_u} = b$, in the mass flow rate model described by Equation (39), when the valve alters between sonic and subsonic flow regimes; (iii) $x_5 = 0$, in (39), which makes $\dot{m}_1$, $\dot{m}_2$ and u nonsmooth (as the result of discontinuity of Px). To find the numerical value of principal axes length, the extension method of calculating the variational equation of nonsmooth systems (Müller 1995, Kunze 2000) is used. Since all of the states evolve continuously in time, the Jacobian of the transition condition, G, is always the identity matrix. According to (Filippov 1960), the numerical value of variational equations at nonsmooth instants can be defined as:

$$\delta x^+ = G(x^-)\delta x^- + [G(x^-)f_1(x^-) - f_2(x^+)]\frac{H(x^-)\delta x^-}{H(x^-)f_1(x^-)} \tag{B.1}$$

where δx^+ and δx^- are the numerical values of variational equations before and after the nonsmooth instant. f_1 and f_2 are the nonlinear equations of motion before and after the nonsmooth instant, and the plus and minus signs characterize the right and left-sided limits, respectively. The matrix $H(x^-)$ is the Jacobian of the indicator function, $h(x)$, which indicates the switching to the next manifold of motion . Precise examination of the Equation (31) shows that the right-hand sides of equations never experience discontinuity. In other words, $f_1 = f_2 = f$, and (B.1) yields:

$$\delta x^+ = \delta x^- \tag{B.2}$$

At the nonsmooth instants of motion, where Jacobian does not exist, Equation (B.2) can be used.